Journal of Nanophotonics

Nanophotonics.SPIEDigitalLibrary.org

Theoretical investigation of a plasmonic sensor based on a metal–insulator–metal waveguide with a side-coupled nanodisk resonator

Yiyuan Xie
Yexiong Huang
Hongjun Che
Weilun Zhao
Weihua Xu
Xin Li
Jiachao Li

SPIE.

Theoretical investigation of a plasmonic sensor based on a metal–insulator–metal waveguide with a side-coupled nanodisk resonator

Yiyuan Xie,* Yexiong Huang, Hongjun Che, Weilun Zhao, Weihua Xu, Xin Li, and Jiachao Li
Southwest University, College of Electronic and Information Engineering, No. 2 Tiansheng Road, BeiBei District, Chongqing 400715, China

Abstract. A plasmonic sensor based on a metal–insulator–metal waveguide with a side-coupled nanodisk resonator is proposed and numerically investigated using a finite-difference time-domain method. The numerical simulation results indicate that more than one sharp resonance dip appears in the transmission spectrum in the telecommunication regime, and each resonance wavelength has a linear relationship with the refractive index of the dielectric in the resonator. In addition, the sensing characteristics of the structure and the influence of its structural parameters are analyzed in detail by investigating the transmission spectra. As a refractive-index sensor, its sensitivity can reach as high as 1150 nm per refractive index unit near the resonance wavelength of 1550 nm, and its sensing resolution can reach 10^{-6} for a wavelength resolution of 0.01 nm. Furthermore, by employing the relationship between the temperature and the refractive index, the temperature-sensing characteristics of the structure are also discussed. Near the resonance wavelength of 1550 nm, the temperature sensitivity can reach 0.45 nm/°C. The sensor has a compact and simple structure and may find many potential and important applications in optical networks-on-chip and on-chip nanosensors. © *2015 Society of Photo-Optical Instrumentation Engineers (SPIE)* [DOI: 10.1117/1.JNP.9.093099]

Keywords: surface plasmon polaritons; plasmonic sensor; nanodisk resonator; refractive index; temperature; finite-difference time-domain method.

Paper 14146 received Nov. 17, 2014; accepted for publication Dec. 18, 2014; published online Jan. 13, 2015.

1 Introduction

Compared with a conventional electrical sensor, an optical sensor has many significant advantages, such as immunity to electromagnetic interference, great sensitivity, and a wide dynamic range.[1–3] In particular, optical sensors based on surface plasmon resonance (SPR) have received great attention for their optical properties, including a local electromagnetic field enhancement and the ultrasensitivity of the SPR to the surrounding medium.[4–8] To satisfy the increasing needs of high integration and high sensitivity for optical sensors, an SPR sensor based on propagating surface plasmon polaritons (SPPs) can be a good and promising candidate. SPPs are surface electromagnetic waves excited at the metal–dielectric interface. The surface electromagnetic wave propagates along the interface, and its field amplitude decays exponentially on both sides of the interface, which is attributed to the interaction between the surface charge oscillation of free electrons and the electromagnetic field. Its specific properties of overcoming the diffraction limit for light waves and guiding light waves at subwavelength scales help to further miniaturize integrated photonic devices and circuits.[9–12] Additionally, compared with an insulator–metal–insulator waveguide, a metal–insulator–metal (MIM) waveguide has been shown to be the most efficient structure for guiding SPP waves because it can exhibit strong light confinement and has an acceptable propagation length for SPP propagation.[13–17] SPP sensors can be

*Address all correspondence to: Yiyuan Xie, E-mail: yyxie@swu.edu.cn

realized mainly owing to their extremely sensitive resonance spectral response to changes in the refractive index of the dielectric medium.[7,18] Therefore, SPP sensors not only have the advantage of high sensitivity but also have high integration. In recent years, novel SPP sensors with different structures have been designed and numerically investigated for their sensing applications.[3,18–20] These structures include a simple nanodisk resonator, the coupling of a split waveguide mode with a cavity mode, and a plasmonic waveguide with a coupled ring resonator. Accordingly, the related theoretical results on the sensing characteristics and the applications of SPP sensors have been reported. We note that most efforts have focused on numerical investigations of refractive-index sensing. Although refractive-index sensing is very important, temperature sensing is also very valuable for SPP sensors in sensor networks-on-chip. However, studies on temperature sensing are still relatively inadequate.

In this paper, to our best knowledge, we first report theoretical research on the sensing characteristics of a plasmonic sensor based on an MIM waveguide and a side-coupled nanodisk resonator. A finite-difference time-domain (FDTD) method is used to investigate the transmission characteristics of the proposed sensor. In addition, the refractive-index sensing characteristics of the proposed sensor are investigated in detail, and its temperature-sensing characteristics are studied by investigating the transmission spectra in the telecommunication regime. The results can provide a theoretical foundation for research on compact sensors applied in optical sensor networks, on-chip nanosensors, and so on.

2 Model Structure and Theoretical Analysis

Figure 1 shows a two-dimensional schematic diagram of the proposed structure of the plasmonic sensor consisting of an MIM waveguide and a side-coupled nanodisk resonator. The nanodisk resonator is located on one side of the MIM waveguide at a coupling distance. The dimensional parameters of the structure R, w, and d are the radius of the nanodisk resonator, the width of the waveguide, and the coupling distance between the nanodisk cavity and the MIM waveguide, respectively. The MIM waveguide is set to be air, and the nanodisk cavity is filled with a dielectric material with a refractive index n_d. The metal is assumed to be silver, which has a frequency-dependent permittivity given by the well-known Drude model:

$$\varepsilon_m(\omega) = \omega_\infty - \frac{\omega_p^2}{\omega(\omega + i\omega_c)}, \tag{1}$$

where ε_∞, ε_p, ω_c, and ω are the dielectric constant at infinite frequency, the bulk plasma frequency, the electron collision frequency, and the angular frequency of the incident wave, respectively. For silver, these parameters have the following values: $\varepsilon_\infty = 3.7$, $\varepsilon_p = 9.1$ eV, and $\omega_c = 0.018$ eV.[15]

The SPP waves are excited by the transverse magnetic (TM) mode on the left side of the waveguide (only TM-polarized light can excite an SPP wave). When a wave propagates along the MIM waveguide from the input port to the output port, part of the energy will be coupled to the nanodisk resonator, and a standing wave can be formed in the resonator, producing a resonance dip in the transmission spectrum at the resonance wavelength. The resonance condition should satisfy the following relationship:

$$k_d \frac{H_n^{(1)\prime}(k_m R)}{H_n^{(1)}(k_m R)} = k_m \frac{J_n'(k_d R)}{J_n(k_d R)}, \tag{2}$$

where $k_m = k\sqrt{\varepsilon_m}$ and $k_d = k\sqrt{\varepsilon_d}$ represent the wave vectors of the metal and dielectric medium, respectively. $k = 2\pi/\lambda$ is the wave vector of the incident electromagnetic wave in free space. ε_m and ε_d are the relative permittivities of the metal and dielectric medium, respectively. J_n and J_n' are a Bessel function of the first kind with order n and its derivative, respectively; similarly, $H_n^{(1)}$ and $H_n^{(1)\prime}$ are a Hankel function of the first kind with order n and its derivative, respectively.[16–21] According to Eq. (2), the resonance frequency is a function of the radius of the disk and the refractive index n_d (i.e., $\sqrt{\varepsilon_d}$) of the dielectric in the resonator.

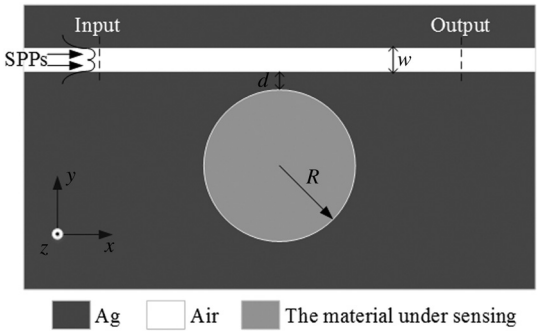

Fig. 1 Schematic diagram of the plasmonic sensor based on a metal–insulator–metal (MIM) waveguide with a side-coupled nanodisk resonator. R is the radius of the nanodisk resonator, w is the width of the MIM waveguide, and d is the coupling distance between the resonator and the MIM waveguide.

The transmission characteristic T is determined by the relationship $T = P_{\text{out}}/P_{\text{in}}$ (P_{in} and P_{out} are the powers at the input and output ports, respectively), which can be described by the following equation:

$$T(\omega) = 1 + \frac{(1/\tau_i)^2 - (1/\tau_i + 1/\tau_w)^2}{(\omega - \omega_0)^2 + (1/\tau_i + 1/\tau_w)^2}, \tag{3}$$

where ω_0 is the resonance frequency. $1/\tau_i$ is the decay rate of the power due to the internal loss in the disk resonator, and $1/\tau_w$ is the decay rate of the escaped power coupled into the waveguide from the disk resonator.[16,17] As can be deduced from Eq. (3), a minimum value $T_{\text{min}} = (1/\tau_i)^2/(1/\tau_i + 1/\tau_w)^2$ will appear in the transmission spectrum if the incident frequency is equal to the resonance frequency (i.e., $\omega = \omega_0$).

In this study, we want to investigate the temperature-sensing characteristics of the proposed structure. From the above analysis, we note that it is relevant between the refractive index and the resonance wavelength. To the best of our knowledge, the refractive index is related to the surrounding temperature. As a temperature sensor, a material with a high refractive-index temperature coefficient should be used as the sensing medium. In this study, we choose ethanol as the sensing medium in the resonator because it has a high refractive-index temperature coefficient of 3.94×10^{-4}. The relationship between the refractive index n and the temperature T of ethanol is

$$n = 1.36836 - 3.94 \times 10^{-4}\ \text{T}. \tag{4}$$

Equation (4) indicates that there is a linear relationship between the refractive index and the temperature, resulting in the same relationship between the temperature and the resonance wavelength.[18,20] Therefore, the temperature can be obtained by detecting the shift in the resonance wavelength.

3 Simulation Results and Discussions

In order to investigate the transmission characteristics, the transmission properties of the structure are simulated by an FDTD method. Figure 2(a) shows the transmission spectrum of the structure in the incident wavelength range from 400 to 2200 nm. The structural parameters are set to be $R = 295$ nm, $d = 15$ nm, $w = 30$ nm, and $n_d = 1.36048$ so that a resonance wavelength could be obtained near 1550 nm. Here, $n_d = 1.36048$ is the refractive index of ethanol at room temperature ($T = 20$°C). As shown in Fig. 2(a), four very sharp resonance dips appear in the transmission spectrum at wavelengths of $\lambda_0 = 1550$, 964.2, 728.3, and 600.7 nm, which correspond to the resonance modes of mode I ($n = 1$), mode II ($n = 2$), mode III ($n = 3$), and mode IV ($n = 4$), respectively. The longest distance of 585.8 nm occurs between the resonance wavelengths of mode I and mode II, which is important to the measurement regime of the sensor. Figures 2(b)–2(f) show the contour profiles of the field distributions of $|H_z|$ for incident

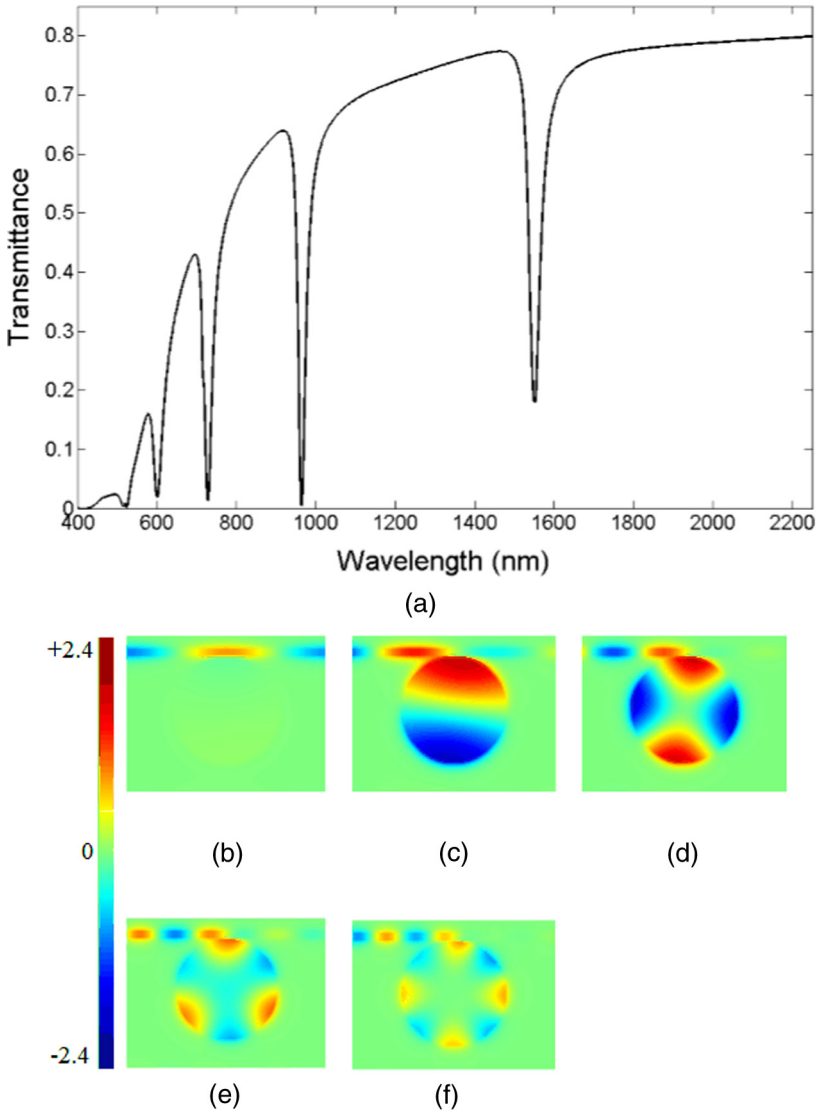

Fig. 2 (a) Simulated transmission spectrum of the structure with $R = 295$ nm, $d = 15$ nm, $w = 30$ nm, and $n_d = 1.36048$. The contour profiles of the field distributions of $|H_z|$ at different incident wavelengths of (b) 2000 nm, (c) 1550 nm, (d) 964.2 nm, (e) 728.3 nm, and (f) 600.7 nm.

wavelengths of 2000, 1550, 964.2, 728.3, and 600.7 nm, respectively. As can be observed in Figs. 2(b)–2(f), most of the energy of the incident waves is coupled to the resonator, and the corresponding standing waves are formed in the resonator at the resonance wavelengths. However, the incident wave can be barely coupled to the resonator and propagated to the right side of the MIM waveguide at a wavelength of 2000 nm, which is consistent with the results observed from the transmission spectrum.

In order to investigate the relationship between the refractive index of the dielectric in the resonator and the resonance wavelength of the structure, the resonator is filled with a dielectric having a refractive index increasing from 1.26 to 1.48 in steps of 0.02, while the other parameters are fixed at $R = 295$ nm, $d = 15$ nm, and $w = 30$ nm. Figure 3(a) shows the transmission spectra for these conditions. As can be observed in Fig. 3(a), all resonance wavelengths exhibit a redshift, and new resonance dips appear at short wavelengths as the refractive index increases. In this study, we consider only modes I to IV. When the refractive index increases from 1.26 to 1.48, the resonance wavelength has shifts of 253 nm for mode I, 155.6 nm for mode II, 116.6 nm for mode III, and 96.2 nm for mode IV. Figure 3(b) shows the linear relationships between the resonance wavelength and the refractive index for the different modes in the range of variation.

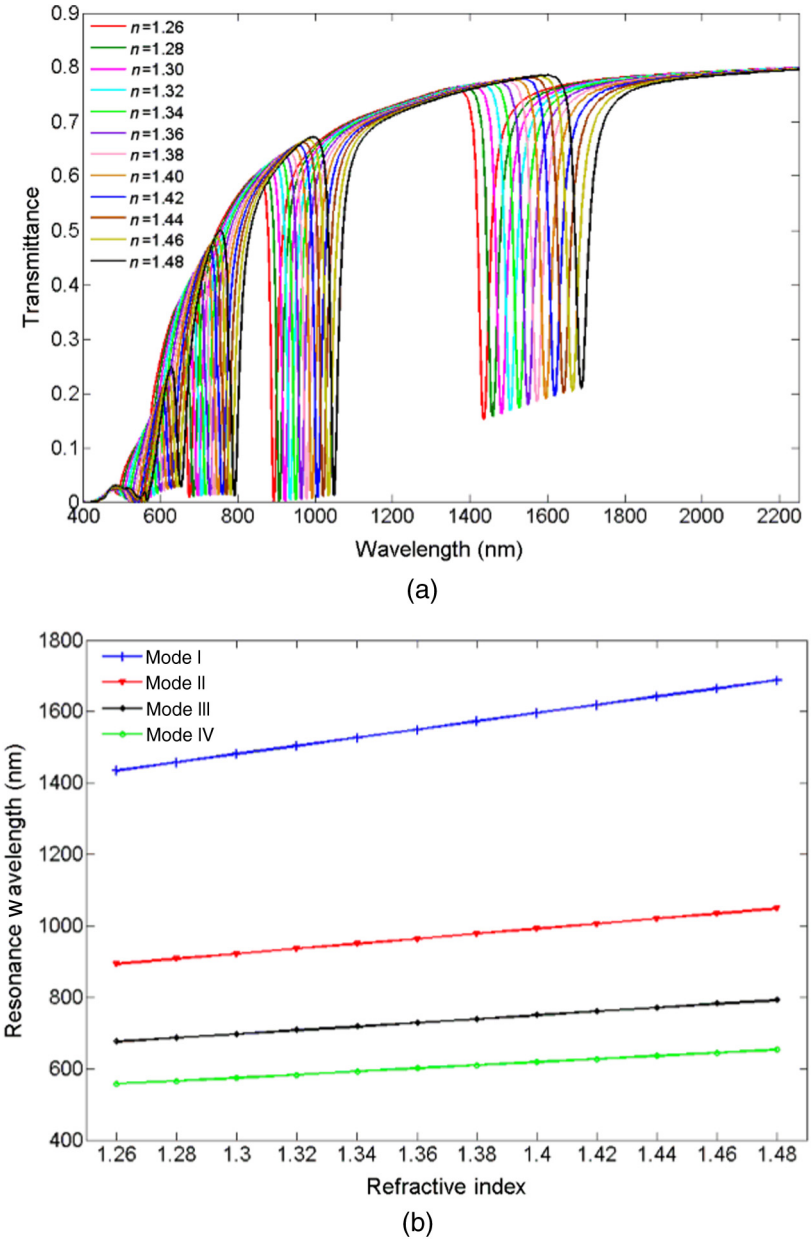

Fig. 3 (a) Transmission spectra of the structure with different refractive indices from 1.26 to 1.48. (b) Resonance wavelength as a function of the refractive index of the dielectric in the resonator for the different modes.

Therefore, the refractive index can be obtained by measuring the shift in a certain resonance wavelength based on this linear relationship. This is the sensing principle of the proposed structure as a sensor. Furthermore, the performance of a sensor can be evaluated by its sensitivity (S) and sensing resolution (SR).[5,22] The sensitivity of the sensor is defined as the shift in the resonance wavelength per unit variation in the refractive index (i.e., $S = \Delta\lambda/\Delta n$), and the sensing resolution is defined as $SR = (dn/d\lambda)\Delta\lambda$.[19,21] According to the definition, the sensitivities of the sensor can reach 1150 nm/refractive-index unit (RIU) for mode I, 707.3 nm/RIU for mode II, 530 nm/RIU for mode III, and 437.3 nm/RIU for mode IV. Accordingly, the sensing resolutions of the sensor will reach as high as 8.7×10^{-6} for mode I, 1.4×10^{-5} for mode II, 1.89×10^{-5} for mode III, and 2.29×10^{-5} for mode IV, given a wavelength detection resolution of $\Delta\lambda = 0.01$ nm, which a high-resolution optical spectrum analyzer can achieve.[19] According to the above analysis, the proposed sensor not only has a high sensitivity for refractive-index sensing, but also a high sensing resolution.

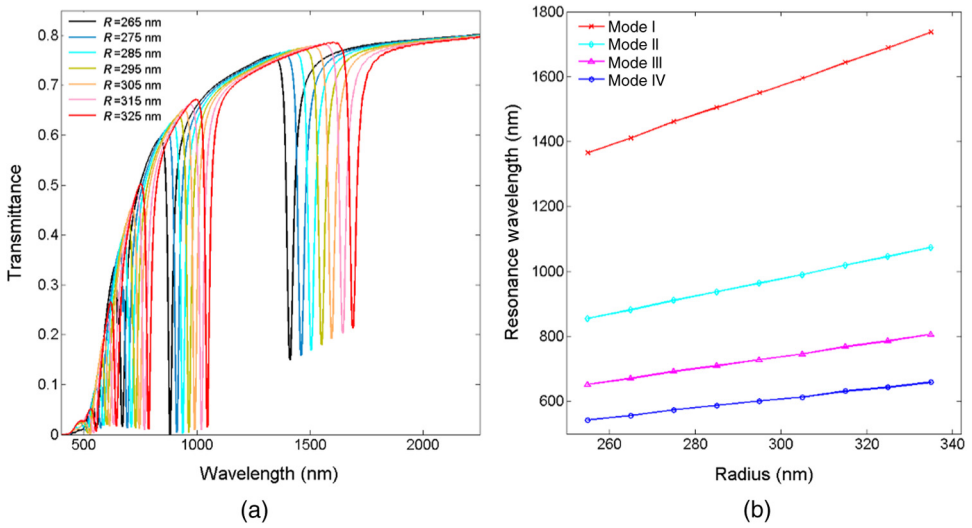

Fig. 4 (a) Transmission spectra of the structure for different radii. (b) Resonance wavelength as a function of the radius.

Successively, we investigate how the structural parameters affect the transmission and sensing characteristics of the sensor. First, we investigate how the radius of the resonator affects the transmission and sensing characteristics by increasing R from 265 to 325 nm in 10-nm steps while the other parameters are fixed at $d = 15$ nm, $w = 30$ nm, and $n_d = 1.36048$. Figure 4(a) shows the transmission spectra of the sensor for different radii. As shown in Fig. 4(a), all resonance wavelengths shift to larger wavelengths with an increase in the radius. Figure 4(b) shows the resonance wavelength of each mode as a function of the radius of the disk resonator. In Fig. 4(b), the resonance wavelength has an approximately linear relationship with the radius.

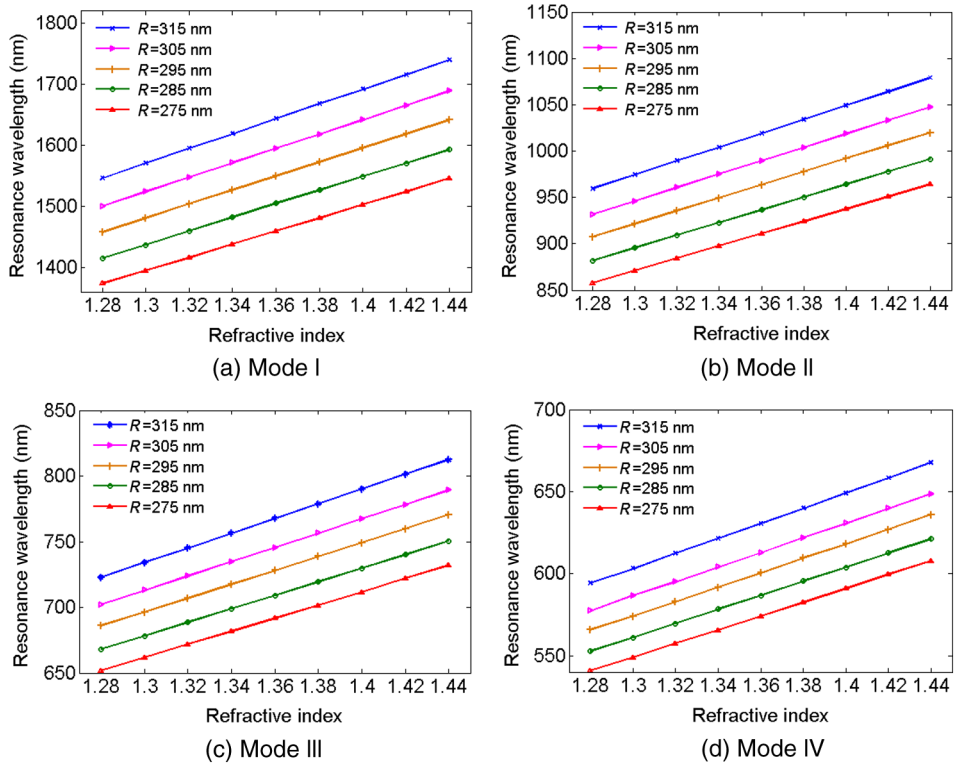

Fig. 5 Resonance wavelength of the structure as a function of the refractive index for different radii for (a) mode I, (b) mode II, (c) mode III, and (d) mode IV.

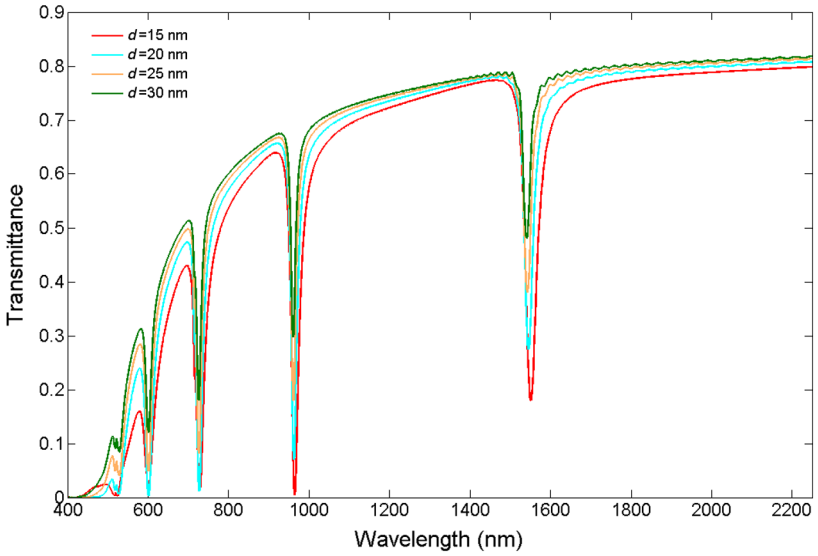

Fig. 6 Transmission spectra of the structure for different coupling distances.

The resonance wavelength of mode I is the most sensitive to a change in the radius, which has a slope of 4.63. In order to illustrate how the radius affects the refractive-index sensing characteristics, we change the refractive index for different radii of 275, 285, 295, 305, and 315 nm. Figure 5 shows the relationship between the resonance wavelength and the refractive index for different radii for each mode. According to the analysis and calculation, we can conclude that the sensitivity increases as the radius increases, and mode I is more sensitive to the radius than the other modes. This is mainly attributed to the rate of change in the resonance wavelength as the radius increases. However, the resonance wavelength becomes larger when the radius

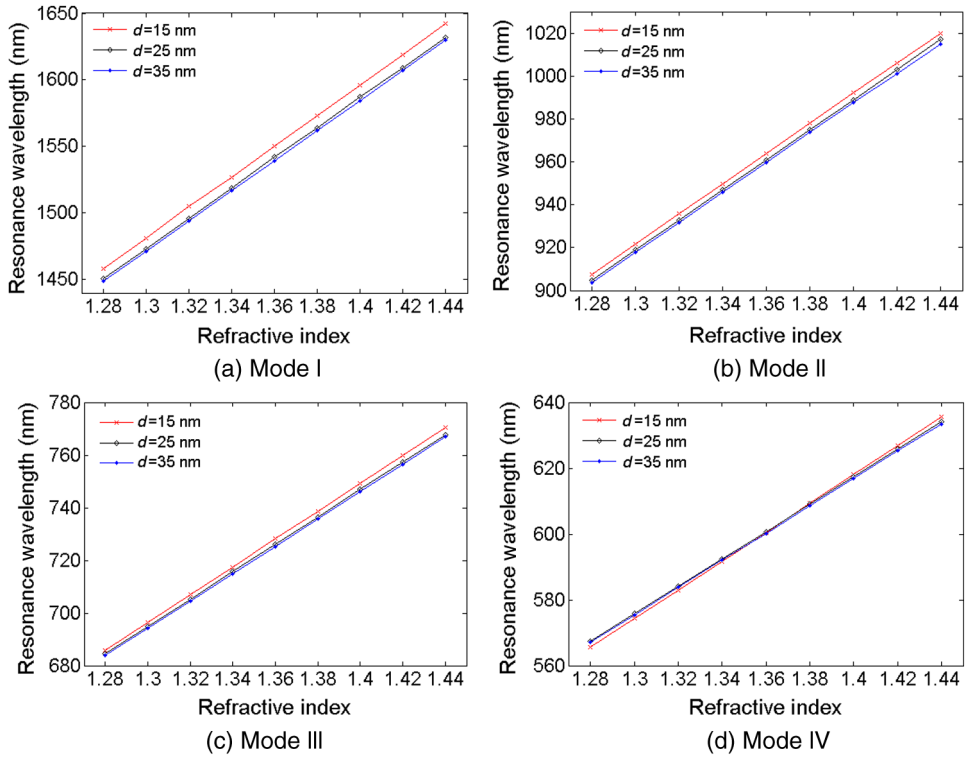

Fig. 7 Resonance wavelength of the structure as a function of the refractive index for different coupling gaps for (a) mode I, (b) mode II, (c) mode III, and (d) mode IV.

increases. From the above analysis, the resonance wavelength and the sensitivity of the sensor can be tuned by changing the radius of the cavity.

Next, to analyze the effect of the coupling distance on the transmission and sensing characteristics, d is increased from 15 to 30 nm in 5-nm steps while the other parameters are fixed at $R = 295$ nm, $w = 30$ nm, and $n_d = 1.36048$. Figure 6 shows the transmission spectra for different coupling distances of 15, 20, 25, and 30 nm. As shown in Fig. 6, all resonance wavelengths of each mode exhibit a slight blueshift as the coupling distance increases. On the other hand, the

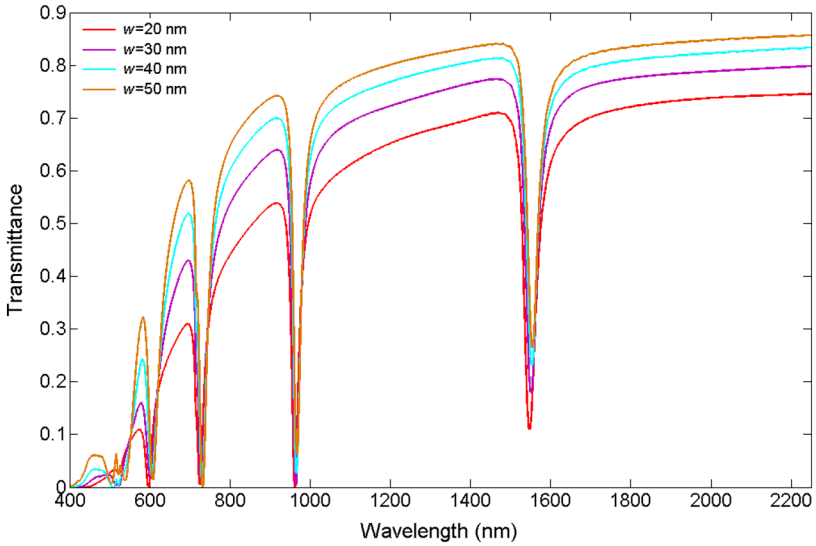

Fig. 8 Transmission spectra of the structure for different waveguide widths.

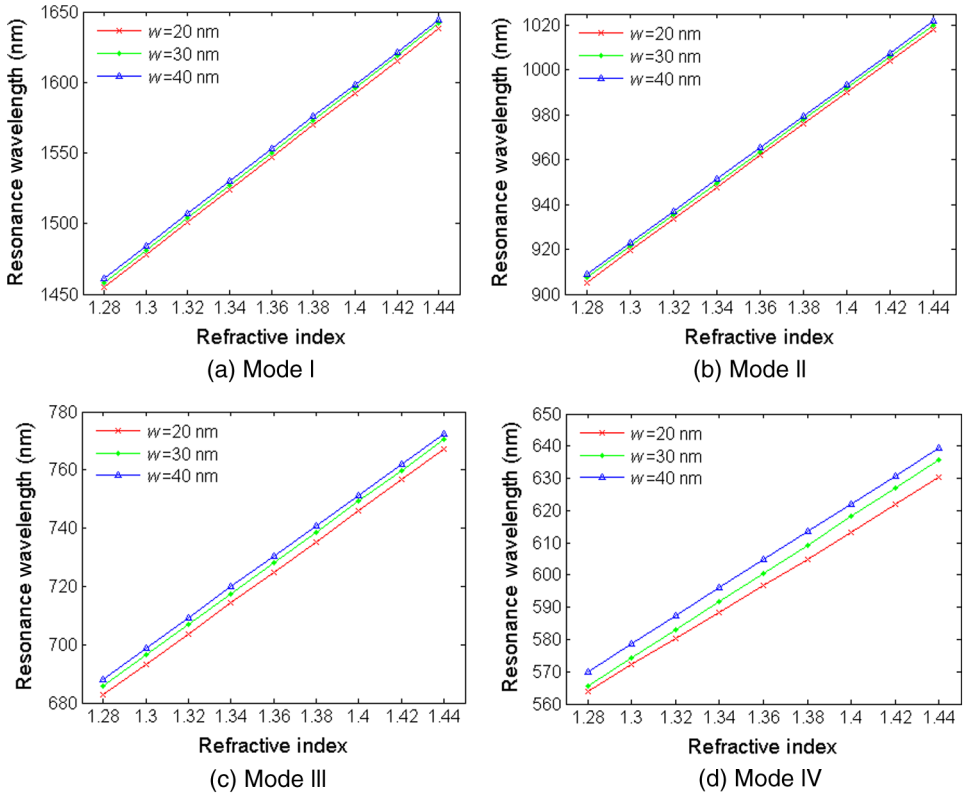

Fig. 9 Resonance wavelength of the structure as a function of the refractive index for different waveguide widths for (a) mode I, (b) mode II, (c) mode III, and (d) mode IV.

transmittance becomes larger, and the dips become narrower at the resonance wavelength when the coupling distance increases. This could be explained by temporal coupled-mode theory.[16] To display how the coupling distance affects the sensing characteristics, we only change the refractive index for different coupling distances of 15, 25, and 35 nm while the other parameters are fixed. Figure 7 shows the resonance wavelength versus the refractive index for different coupling distances for each mode. According to the analysis and calculation, the sensitivities are 1131.2 nm/RIU for mode I, 695.62 nm/RIU for mode II, 518.125 nm/RIU for mode III, and 413.75 nm/RIU for mode IV when $d = 35$ nm. Furthermore, the sensitivities are 1131.25 nm/RIU for mode I, 700.625 nm/RIU for mode II, 520 nm/RIU for mode III, and 417.5 nm/RIU for mode IV when $d = 25$ nm. As can be concluded, the coupling distance affects not only the resonance wavelength but also the sensitivity. The sensitivity becomes smaller as the coupling distance increases for each mode; however, it has little influence on the sensing characteristics when $d = 25$ and 35 nm. Therefore, the structure can be optimized by changing the coupling distance.

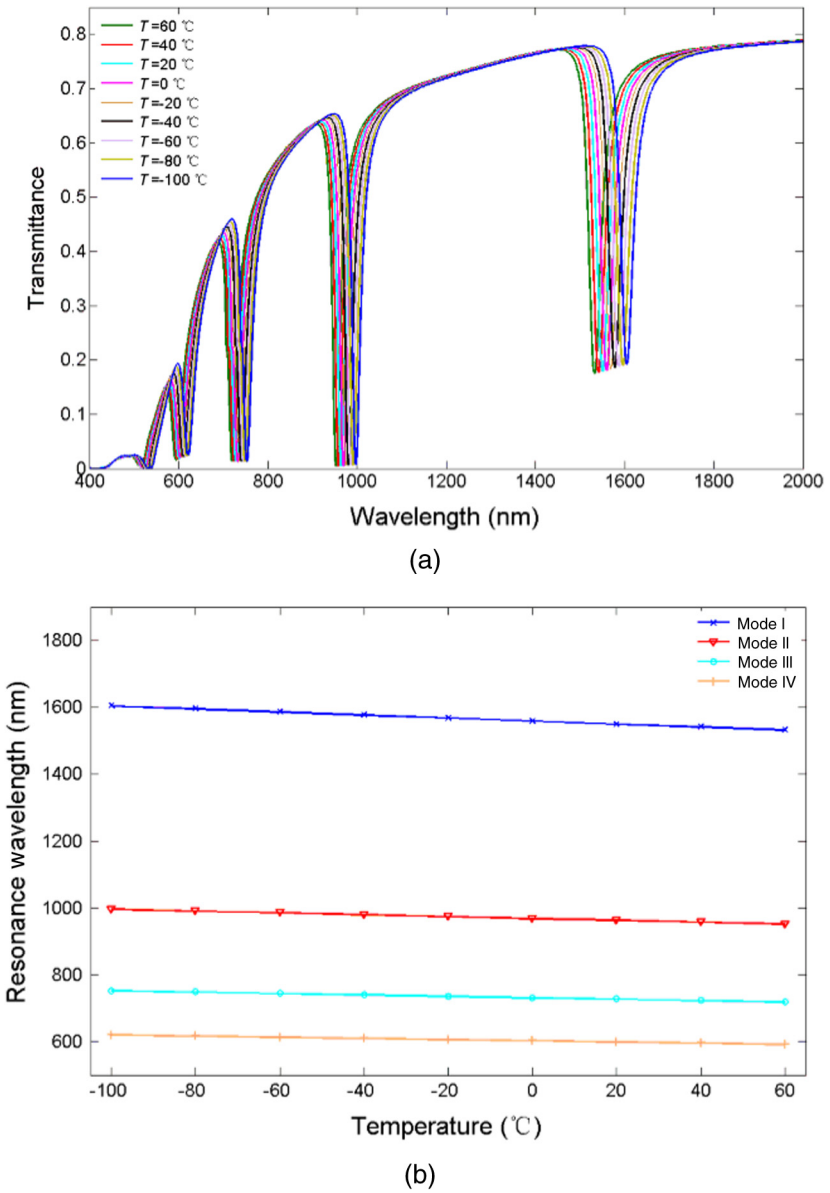

Fig. 10 (a) Transmission spectra of the structure for different temperatures. (b) Resonance wavelength as a function of the temperature for the different modes.

In order to study the influence of the waveguide width on the transmission and sensing characteristics, w is increased from 20 to 50 nm in 10-nm steps while the other parameters are fixed at $R = 295$ nm, $d = 15$ nm, and $n_d = 1.36048$. Figure 8 shows the transmission spectra for different waveguide widths of 20, 30, 40, and 50 nm. The resonance wavelength exhibits a slight redshift as the waveguide width increases; however, the transmittance evidently becomes larger as the waveguide width increases. This may be attributed to the waveguide loss. The increase of the width of the waveguide decreases the coupling of SPPs and reduces the waveguide loss. As a result, this will affect the coupling effect between the waveguide and the cavity and result in a slight redshift of the resonance wavelength.[23] To investigate how the waveguide width affects the sensing characteristics, we change the refractive index for different waveguide widths of 20, 30, and 40 nm while the other parameters are fixed. Figure 9 shows the relationship between the resonance wavelength and the refractive index for different waveguide widths for each mode. According to the analysis and calculation, the sensitivities are 1143.75 nm/RIU for mode I, 704.375 nm/RIU for mode II, 526.25 nm/RIU for mode III, and 415.625 nm/RIU for mode IV when $w = 20$ nm. Further, the sensitivities are 1143.75 nm/RIU for mode I, 707.5 nm/RIU for mode II, 527.5 nm/RIU for mode III, and 434.375 nm/RIU for mode IV when $w = 40$ nm. As can be observed in Fig. 9, the waveguide width has a different influence on the sensing characteristics for different modes. Compared with the sensitivities of mode I and mode IV, the sensitivities of mode II and mode III are weakly affected. However, it has a relatively good sensitivity at $w = 30$ nm. Therefore, the structure can also be optimized by changing the waveguide width, similar to the coupling distance.

Finally, the temperature-sensing characteristics of the structure were analyzed. In order to investigate the relationship between the resonance wavelength and the temperature, we increase the temperature of ethanol from −100 to 60°C in steps of 10°C according to Eq. (4) while the other structural parameters are fixed at $R = 295$ nm, $d = 15$ nm, and $w = 30$ nm. Figure 10(a) shows the transmission spectra for different temperatures, in which the resonance wavelength exhibits a slight blueshift as the temperature increases. This is because the refractive index of

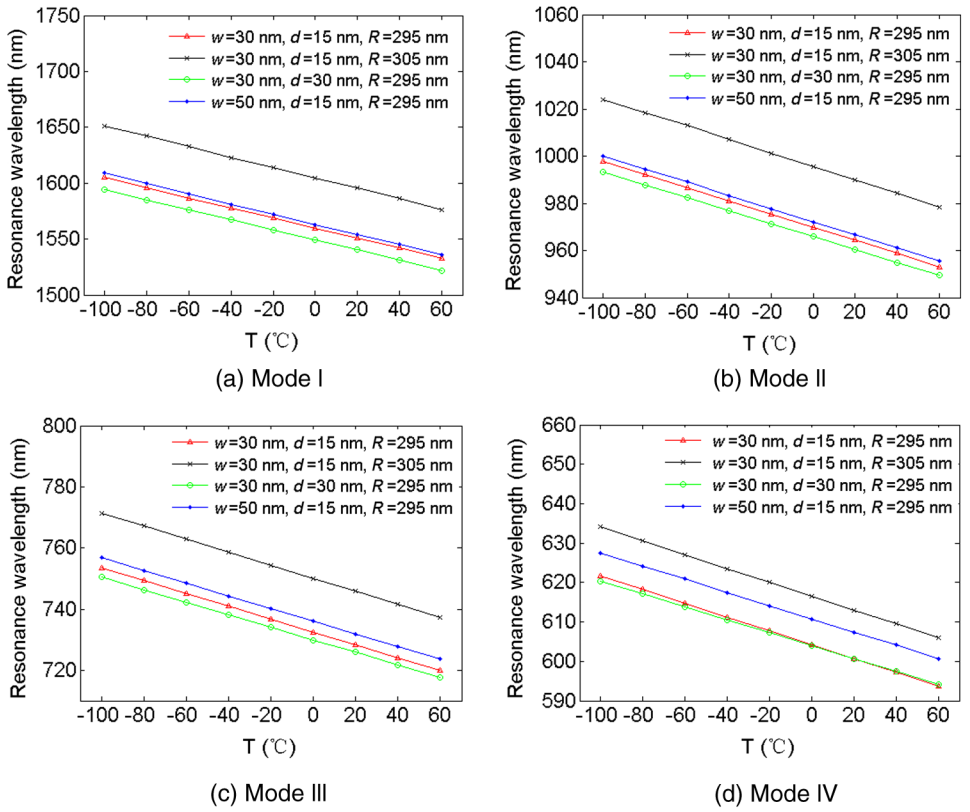

Fig. 11 Resonance wavelength of the structure as a function of temperature for different structural parameters for (a) mode I, (b) mode II, (c) mode III, and (d) mode IV.

ethanol decreases as the temperature increases. Figure 10(b) shows the linear relationship between the resonance wavelength and the temperature. The sensitivity of the temperature sensor is defined[24] as $d\lambda/dT$, resulting in 0.45 nm/°C for mode I, 0.28 nm/°C for mode II, 0.21 nm/°C for mode III, and 0.17 nm/°C for mode IV. To study the influence of different structural parameters on the sensing characteristics, Fig. 11 shows the relationship between the resonance wavelength and the temperature for different structural parameters for each mode. The temperature sensitivities of the structure with $w = 30$ nm, $d = 15$ nm, and $R = 305$ nm are 0.46875 nm/°C for mode I, 0.284 nm/°C for mode II, 0.214 nm/°C for mode III, and 0.176 nm/°C for mode IV. Further, the temperature sensitivities with $w = 30$ nm, $d = 30$ nm, and $R = 295$ nm are 0.45 nm/°C for mode I, 0.275 nm/°C for mode II, 0.204 nm/°C for mode III, and 0.163 nm/°C for mode IV. In addition, the temperature sensitivities with $w = 50$ nm, $d = 15$ nm, and $R = 295$ nm are 0.456 nm/°C for mode I, 0.279 nm/°C for mode II, 0.2075 nm/°C for mode III, and 0.1675 nm/°C for mode IV. Therefore, we can optimize the temperature sensor by tuning the structural parameters. In particular, the temperature sensitivity can be evidently improved by increasing the radius of the resonator, as for the refractive-index sensor.

4 Conclusion

In conclusion, a plasmonic sensor is proposed and numerically investigated using an FDTD method in the telecommunication regime. The structure of the sensor is based on an MIM waveguide with a side-coupled disk cavity. Based on the relationship among the resonance wavelength, the refractive index of the dielectric in the resonator, and the temperature, the structure is analyzed for refractive-index and temperature sensing by investigating the transmission spectra. The refractive-index and temperature sensitivities can reach as high as 1150 nm/RIU and 0.45 nm/°C near the resonance wavelength of 1550 nm, respectively. In addition, the sensing resolution can reach 10^{-6} for a wavelength resolution of 0.01 nm. Furthermore, the effects of the structural parameters on the sensing characteristics are also investigated in detail. The structure can be optimized by tuning the waveguide width, coupling distance, and the radius of the resonator to improve the performance. The results can provide a theoretical foundation for research on compact sensors applied in optical sensor networks, on-chip nanosensors, and so on.

Acknowledgments

This work was supported in part by the National Natural Science Foundation of China under Grant Numbers 61205088, 61170248, 61373179, and 61373178, in part by the Natural Science Foundation of Chongqing Municipal under Grant Number 2011BB2009, and in part by the Fundamental Research Funds for the Central Universities under Grant Numbers XDJK2014A017, XDJK2013A018, and 2362014XK12.

References

1. V. K. Rai, "Temperature sensors and optical sensors," *Appl. Phys. B* **88**(2), 297–303 (2007).
2. G. D. Kim et al., "Silicon photonic temperature sensor employing a ring resonator manufactured using a standard CMOS process," *Opt. Express* **18**(21), 22215–22221 (2010).
3. A. Dolatabady, N. Granpayeh, and V. F. Nezhad, "A nanoscale refractive index sensor in two dimensional plasmonic waveguide with nanodisk resonator," *Opt. Commun.* **300**, 265–268 (2013).
4. L. M. Tong et al., "Recent advances in plasmonic sensors," *Sensors* **14**(5), 7959–7973 (2014).
5. S. Roh, T. Chung, and B. Lee, "Overview of the characteristics of micro-and nanostructured surface plasmon resonance sensors," *Sensors* **11**(12), 1565–1588 (2011).
6. J. Homola, "Present and future of surface plasmon resonance biosensors," *Anal. Bioanal. Chem.* **377**(3), 528–539 (2003).

7. K. S. Sachin and D. G. Banshi, "Fiber optic plasmonic sensors: past, present and future," *Open Opt. J.* **7**, 58–83 (2013).
8. J. H. Ahn et al., "Fiber-optic waveguide coupled surface plasmon resonance sensor," *Opt. Express* **20**(19), 21729–21738 (2012).
9. W. L. Barnes, A. Dereux, and T. W. Ebbesen, "Surface plasmon subwavelength optics," *Nature* **424**(6950), 824–830 (2003).
10. D. K. Gramotnev and S. I. Bozhevolnyi, "Plasmonics beyond the diffraction limit," *Nat. Photonics* **4**(2), 83–91 (2010).
11. S. A. Maier and H. A. Atwater, "Plasmonics: localization and guiding of electromagnetic energy in metal/dielectric structures," *J. Appl. Phys.* **98**(1), 011101 (2005).
12. H. Ditlbacher et al., "Two-dimensional optics with surface plasmon polaritons," *Appl. Phys. Lett.* **81**(10), 1762–1764 (2002).
13. H. Lu et al., "Analysis of nanoplasmonic wavelength demultiplexing based on metal-insulator-metal waveguides," *J. Opt. Soc. Am. B* **28**(7), 1616–1621 (2011).
14. H. Lu et al., "Tunable band-pass plasmonic waveguide filters with nanodisk resonators," *Opt. Express* **18**(17), 17922–17927 (2010).
15. G. Wang et al., "Tunable multi-channel wavelength demultiplexer based on MIM plasmonic nanodisk resonators at telecommunication regime," *Opt. Express* **19**(4), 3513–3518 (2011).
16. H. Lu et al., "Multi-channel plasmonic waveguide filters with disk-shaped nanocavities," *Opt. Commun.* **284**(10–11), 2613–2616 (2011).
17. F. Lu et al., "A plasmonic triple-wavelength demultiplexing structure based on MIM waveguide with side-coupled nanodisk cavities," *IEEE Trans. Nanotechnol.* **12**(6), 1185–1189 (2013).
18. T. S. Wu et al., "The sensing characteristics of plasmonic waveguide with a single defect," *Opt. Commun.* **323**, 44–48 (2014).
19. X. Jin et al., "A novel nanometeric plasmonic refractive index sensor," *IEEE Trans. Nanotechnol.* **9**(2), 134–137 (2010).
20. T. B. Wang et al., "The transmission characteristics of surface plasmon polaritons in ring resonator," *Opt. Express* **17**(26), 24096–24101 (2009).
21. I. Chremmos, "Magnetic field integral equation analysis of interaction between a surface plasmon polariton and a circular dielectric cavity embedded in the metal," *J. Opt. Soc. Am. A* **26**(12), 2623–2633 (2009).
22. T. Srivastava, R. Das, and R. Jha, "Highly sensitive plasmonic temperature sensor based on photonic crystal surface plasmon waveguide," *Plasmonics* **8**(2), 515–521 (2013).
23. A. Hosseini and Y. Massoud, "Nanoscale surface plasmon based resonator using rectangular geometry," *Appl. Phys. Lett.* **90**(18), 181102 (2007).
24. J. Hu et al., "Influence of temperature on reflectivity of symmetrical metal-cladding optical waveguide," *IEEE Photonics Technol. Lett.* **26**(21), 2166–2169 (2014).

Yiyuan Xie is a professor at Southwest University, Chongqing, China. He received a PhD degree in optical engineering from the Chinese Academy of Science in 2009. He was a visiting scholar with the Hong Kong University of Science and Technology, Hong Kong. He has authored or co-authored more than 30 papers in peer-reviewed journals and international conferences. His current research interests include optical networks-on-chip, ultrahigh optical communications, and optical data centers.

Yexiong Huang is currently working toward an MSc degree at the College of Electronic and Information Engineering, Southwest University, Chongqing, China. His current research interests include surface plasmon polaritons and optical devices.

Hongjun Che is currently working toward an MSc degree at the College of Electronic and Information Engineering, Southwest University, Chongqing, China. His current research interests include the polarization characteristics and nonlinear dynamics of semiconductor lasers and optical communications.

Weilun Zhao is currently working toward an MSc degree at the College of Electronic and Information Engineering, Southwest University, Chongqing, China. His current research

interests include optical networks-on-chip, ultrahigh optical communications, and optical data centers.

Weihua Xu is currently working toward an MSc degree at the College of Electronic and Information Engineering, Southwest University, Chongqing, China. Her current research interests include optical networks-on-chip, ultrahigh optical communications, and optical data centers.

Xin Li is currently working toward an MSc degree at the School of Electronic and Information Engineering, Southwest University, Chongqing, China. Her current research interests include optical networks-on-chip, ultrahigh optical communications, and optical data centers.

Jiachao Li is currently working toward an MSc degree at the College of Electronic and Information Engineering, Southwest University, Chongqing, China. His current research interests include the polarization characteristics and nonlinear dynamics of semiconductor lasers.